Solid State Communications 173 (2013) 30–33

Contents lists available at ScienceDirect

Solid State Communications

journal homepage: www.elsevier.com/locate/ssc

Rectifying property and magnetoresistance of manganite–stannate junctions

Qinzhuang Liu [a], Hong Li [a,*], Bing Li [a], Qiangchun Liu [a], Guangping Zhu [a], Kai Dai [a], Zhongliang Liu [a], Jianjun Liu [a], Jianming Dai [b]

[a] School of Physics and Electronic Information, Huaibei Normal University, Huaibei 235000, PR China
[b] Institute of Solid State Physics, Chinese Academy of Science, Hefei 230031, PR China

ARTICLE INFO

Article history:
Received 7 August 2013
Accepted 25 August 2013
by A.H. MacDonald
Available online 30 August 2013

Keywords:
A. Heterojunctions
A. Magnetically ordered materials
D. Electronic transport

ABSTRACT

By employing the perovskite-structured stannates and manganites, p-$La_{0.67}Ca_{0.33}MnO_3$/i-$SrSnO_3$/n-$La_{0.03}Sr_{0.97}SnO_3$ junctions were fabricated on $SrTiO_3$(001) substrates by pulsed laser deposition technique. The current–voltage curves indicate an excellent rectifying property of the heterojunction in the measurement temperatures from 310 to 10 K. A crossover from negative to positive of magnetoresistance with bias voltage was observed, which was explained by the transport mechanism of diffused electrons.

1. Introduction

Perovskite-structured manganites usually exhibit a rich variety of electronic and magnetic properties due to the strong coupling between charge, spin, and orbital degrees of freedom [1]. Recently, manganite-based heterojunctions have attracted considerable attention in the fabrication of oxide electron devices, because these junctions show the magnetoresistance (MR) of manganites as well as the rectifying behaviors of conventional semiconductor junctions, which have potential applications in spintronics. However, so far, most of the manganite-based p–n or p–i–n junctions were fabricated by growing the manganite films on $SrTiO_3$:Nb substrates [2–7]. To better understand the MR and electrical transport behaviors associated with the band structure at the interface, there is a need to grow the perovskite-structured manganite on other materials to form p–n or p–i–n junctions. Among the doped manganite $La_{1-x}A_xMnO_3$ (A=Ca, Sr, and Ba), the hole doped lanthanum manganite $La_{0.67}Ca_{0.33}MnO_3$ (LCMO) exhibits a colossal magnetoresistance with a ferromagnetic ordering temperature at about 250 K[8]. It would be a suitable choice for practical applications in junctions.

Alkaline earth stannates, having a general formula $ASnO_3$ (A=Ba, Sr, and Ca) and a perovskite structure, are used in a wide variety of electronic devices due to their interesting dielectric and gas-sensing properties [9,10]. Among $ASnO_3$, $SrSnO_3$ (SSO) has a wide band gap of 4.27 eV and a lattice constant of a=4.032 Å [11,12]. They are also usually used as insulating buffer layers in preparation of heterostructures, such as high-critical temperature superconductor $YBa_2Cu_3O_7$ and insulator CeO_2, due to their commensurate lattice parameters [13,14]. More recently, many substitutions at A and Sn sites have been carried out to modify their properties due to their wide band gaps and perovskite structures. Our groups have successfully fabricated transparent and conductive n-type La- and Sb-doped $SrSnO_3$ films [15–17]. In this paper, we report on the fabrication of a LCMO/SSO/$La_{0.03}Sr_{0.97}SnO_3$ p–i–n heterojunction on $SrTiO_3$(001) [STO (001)] substrates by using pulsed laser deposition method, with n-type $La_{0.03}Sr_{0.97}SnO_3$ (LSSO) as a bottom layer, p-type LCMO as the top layer, and SSO as the insulator at middle layer. Excellent rectifying characteristics were observed and the MR effects were investigated.

2. Experiments

LCMO, LSSO, and SSO targets were prepared by standard solid state reactions. LCMO/SSO/LSSO heterostructures were grown on STO(001) substrates by pulsed laser deposition using a KrF 248 nm excimer laser with energy of 300 mJ/pulse at 10 Hz and the target-to-substrate distance of 5.5 cm. For the LCMO/SSO/LSSO p–i–n junctions, the bottom layer LSSO and middle layer SSO were grown at 700 °C in 20 Pa of O_2, and the top layer LCMO films at 740 °C in 10 Pa of O_2. The thicknesses were determined by cross sectional field emission scanning electron microscopy with LCMO, LSSO and SSO layers at about 140 and 90, and 10 nm, respectively, with an accuracy of about ±5%. For comparison, only LCMO and LSSO films were also grown on STO substrates under the same condition. The nominal compositions of the films were assumed to

* Corresponding author. Tel.: +86 561 3803394; fax: +86 561 3803256.
E-mail address: lihonggreat@126.com (H. Li).

0038-1098/$ - see front matter © 2013 Elsevier Ltd. All rights reserved.
http://dx.doi.org/10.1016/j.ssc.2013.08.024

be the same as the targets. The structures of the films were characterized by x-ray diffraction (XRD) using Cu $K\alpha_1$ radiation with $\lambda = 1.5406$ Å (Philips X′pert). The in-plane resistances were measured by the standard four-terminal method on a commercial superconducting quantum interference device (Quantum Design MPMS 5), and the current–voltage (I–V) curves were measured by using the two-probe on the Agilent E5270 I–V parametric measurement system at the temperature range of 310–10 K. The magnetic field was applied parallel to the surface of the films and junctions.

3. Results and discussions

Fig. 1 shows the x-ray $\theta-2\theta$ linear scan on the LCMO/SSO/LSSO/STO(001) heterostructure. Only reflections from the (00l) planes of LCMO, LSSO (SSO) layers, and STO substrates are observed, and no spurious phase or randomly oriented grains appear in the scans, indicating the films exhibit preferred orientation along the c-axis. It should be noted that the diffraction peaks of SSO and LSSO layers overlap due to the low La doping in LSSO films and the same growth condition. The crystalline quality of the films was examined by the x-ray ω-scan rocking curves on the LSSO (002) and LCMO (002) reflections (the inset to Fig. 1), with the full width at half maximum at about 0.086° and 0.49°, respectively, confirming the high crystallinity of the films. The out-of-plane cell constant for the LSSO layers was calculated to be 4.0349 Å, and that was 3.8666 Å for LCMO layer, presenting a lattice mismatch of 4.17% between the two layers.

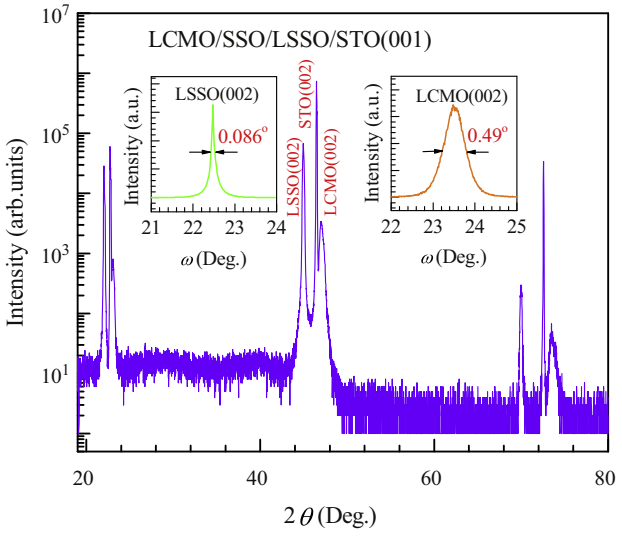

Fig. 1. (Color online) XRD linear scans from the LCMO/SSO/LSSO/STO(001) heterostructures, the insets are the ω-scan rocking curves on the LCMO(002) and LSSO (002) reflections.

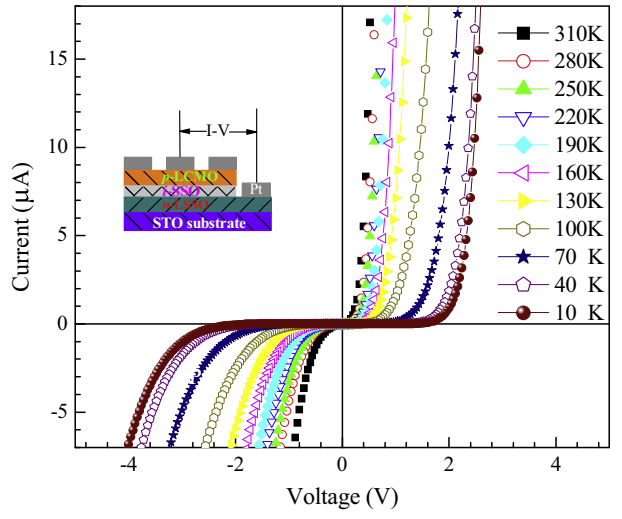

Fig. 2. (Color online) I–V curves of LCMO/SSO/LSSO p–i–n heterojunction at different temperatures. The inset is the schematic illustration of the heterojunction.

Fig. 2 shows the I–V loops of the LCMO/SSO/LSSO junction measured from 310–10 K with an interval of 30 K. The inset is the schematic structure of the p–i–n junction. The Pt electrodes deposited on LCMO and LSSO layer were confirmed to be Ohmic contact. Perfect rectifying characteristics in the temperature range of measurement indicate the formation of the p-LCMO/i-SSO/n-LSSO heterojunction. For a junction, the origin of the rectifying characteristics is the built-in field at the interface of junctions based on the energy band structure of n- and p-type semiconductors [18]. To reduce tunneling current and avoid diffusions, i-layer SSO films were therefore inserted between the n- and p-type semiconductors. There are two critical voltages for the rectifying I–V curves, one is diffusion voltage (V_d), which is defined as the voltage value of the forward current instantaneously increasing. Another is breakdown voltage (V_b), at which the current I starts to increase rapidly at reverse bias. As can be seen in the Fig. 2, both the V_d and the V_b increase with the temperature decreasing from 310 K down to 10 K, which reflects the temperature-dependent variation of Fermi level in LCMO and LSSO films. Similar phenomena were also observed in other manganite-based p–i–n junctions [19,20].

Fig. 3 shows the temperature-dependent resistance of LCMO films and LSSO films grown on STO substrates. As shown in Fig. 3

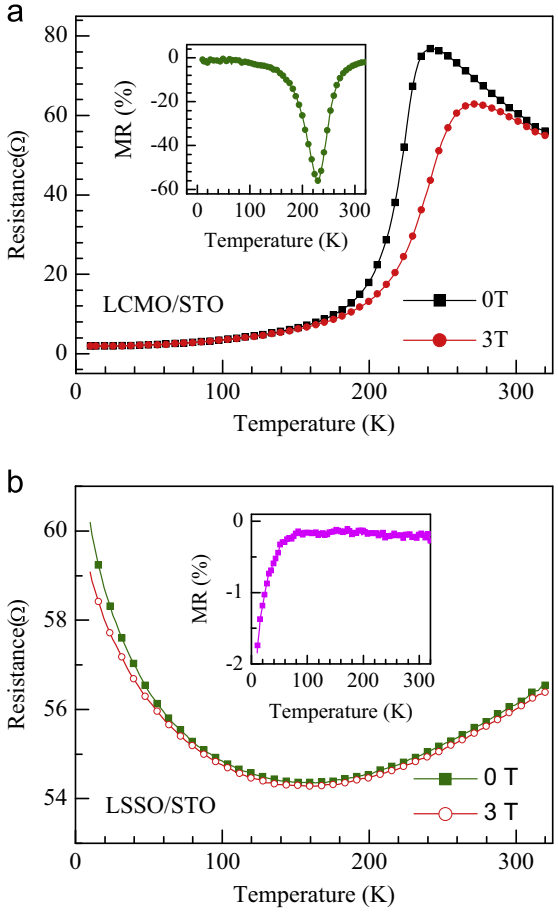

Fig. 3. (Color online) Temperature-dependent resistances of the $La_{0.67}Ca_{0.33}MnO_3$/$SrTiO_3$ films (a) and $La_{0.03}Sr_{0.97}SnO_3$/$SrTiO_3$ films measured at $H=0$ and 3T, insets display the magnetoresistance.

(a), the metal-to-insulator transition temperature of LCMO films appears in 246 K, which is higher than the bulk value of 240 K [1]. Similar to many other manganites, the application of magnetic field (3T) depresses the resistance of LCMO films. Then, a maximal MR of ~56% at 230 K was calculated using the definition of MR=$R(H)/R(0)-1$,with $R(0)$ and $R(H)$ denoting the resistances without and with magnetic field of the films, respectively. As shown in Fig. 3 (b), the LSSO films exhibit a metal-semiconductor transition at 153 K. Hall measurement shows the LSSO films have an *n*-type conductivity with the room-temperature carrier density of 7.6×10^{20} cm^{-3}. The LSSO films exhibit a negligible negative MR in a wide temperature range, and the MR only increases slightly to $-1\sim-2\%$ below 50 K, as shown in inset to Fig. 3(b).

The fascinating characteristics of the manganite-based junction are MR, defined as MR= $(R_H-R_0)/R_0\times100\%$, where R_H is the resistance under magnetic fields, and R_0 is the resistance in zero magnetic field. Fig. 4(a) shows the *I–V* curves of LCMO/SSO/LSSO junction at 280 K under 0 and 3T as a representative phenomenon. It can be seen that the magnetic fields change the current through the junction. The bias voltage dependence of MR at various temperatures was calculated and the results are shown in Fig. 4(b). The sign of MR depends on the applied bias voltage: MR is positive at high bias voltage, and turns to negative at smaller bias voltage. Similar phenomena were also found in $La_{0.7}Ce_{0.3}MnO_3/SrTiO_3$:Nb and $La_{0.82}Ca_{0.18}MnO_3/SrTiO_3$: Nb heterojunctions [21,22].

The crossover of MR from negative to positive with bias voltages of the *p–i–n* junctions can be explained by two different

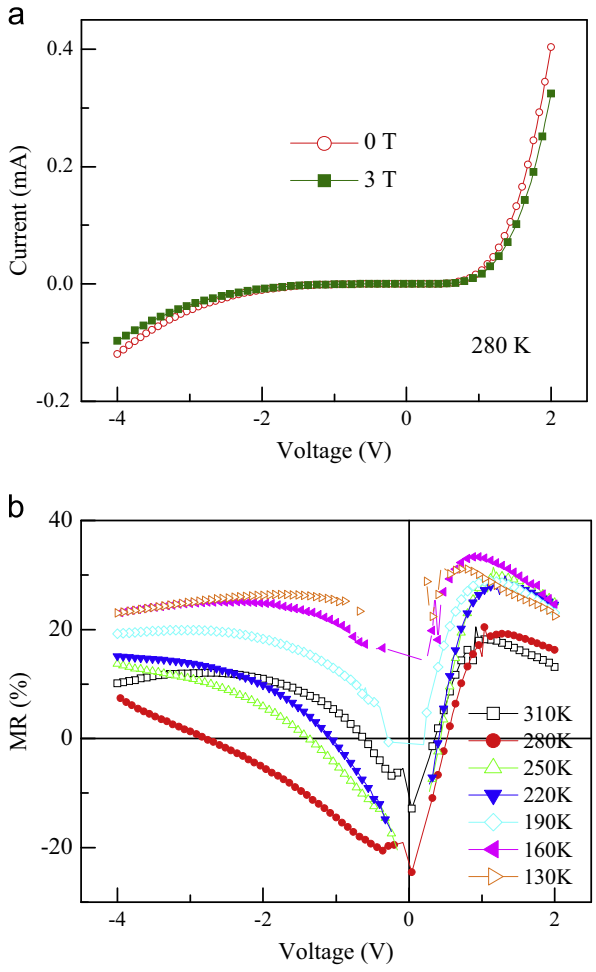

Fig. 4. (Color online) (a) *I–V* curves of the LCMO/SSO/LSSO junction measured at 280 K with magnetic field $H=0$ and 3T, respectively. (b) Voltage dependent MR for LCMO/SSO/LSSO junction.

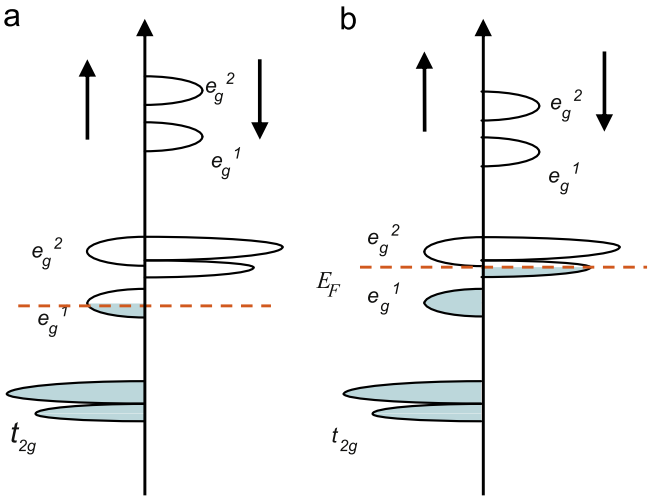

Fig. 5. (Color online) Schematic diagram of spin dependent density of states at low bias voltages (a) and high bias voltages (b)

spin characters of carriers (the majority spin carriers and the minority spin carriers) at the Fermi level E_F. For the band structure of $La_{1-x}Ca_xMnO_3$ material, *d* orbits are split into e_g band and t_{2g} band by the crystal field. Then, the e_g band is divided into e_g^1 and e_g^2 subbands by Jahn–Teller distortion. Moreover, due to the Hund's coupling effect, the e_g band and t_{2g} band are further separated into the spin-up and spin-down bands [21], as schematically shown in Fig. 5. For $La_{0.67}Ca_{0.33}MnO_3$ films, the electrons mainly occupy the lower subband $e_g^{1\uparrow}$, so it exhibits a negative MR within the whole measured temperature range, as shown in the inset to Fig. 3(a). However, for the LCMO/SSO/LSSO heterojunction, when applying low bias voltages, the electrons coming from the LSSO films are limited, and they only fill in the $e_g^{1\uparrow}$ band of LCMO at the interface (Fig. 5 (a)). In this case, the majority spin carriers are still predominant at E_F, and therefore the *p–i–n* junction exhibits a negative MR. While increasing the applied bias voltages, more electrons will be driven from the LSSO films, then the $t_{2g}^{\downarrow}$ band will be occupied, as shown in Fig. 5(b). In this case, the spin orientation of $t_{2g}^{\downarrow}$ electrons is antiparallel to the magnetic moments of the system, consequently resulting in a positive MR [22].

4. Conclusions

In conclusion, using the perovskite-structured SSO and LSSO films as an insulator and n-type semiconductor, respectively, we fabricated the manganite-based *p*-LCMO/*i*-SSO/*n*-LSSO heterojunction by pulsed laser deposition method. The junction demonstrates perfect rectifying characteristic in the whole measurement temperature from 310 to 10 K. The two different spin characters at the Fermi level in the complicated band of $La_{0.67}Ca_{0.33}MnO_3$ might be responsible for the appearance of the MR sign crossover with bias voltage of the *p–i–n* junctions.

Acknowledgments

This work was supported by the Chinese Natural Science Foundation (No. 11004071), and Huaibei Scientific Talent Development Scheme (No. 20130304).

References

[1] Y. Tokura, Colossal Magnetoresistive Oxides (New York: Gordon and Breach) and references therein, 2000.
[2] H. Tanaka, J. Zhang, T. Kawai, Phys. Rev. Lett. 88 (2002) 027204.

[3] M. Wang, D.J. Wang, R.W. Wang, Y.B. Li, Solid State Commun. 170 (2013) 10.
[4] J.R. Sun, C.M. Xiong, T.Y. Zhao, S.Y. Zhang, Y.F. Chen, B.G. Shen, Appl. Phys. Lett. 84 (2004) 1528.
[5] N. Nakagawa, M. Asai, Y. Mukunoki, T. Susaki, H.Y. Hwang, Appl. Phys. Lett. 86 (2005) 082504.
[6] A. Sawa, T. Fujii, M. Kawasaki, Y. Tokura, Appl. Phys. Lett. 86 (2005) 112508.
[7] J. Dho, Solid State Commun. 150 (2010) 2243.
[8] J.M.D. Coey, M. Viret, S. Molnar, Adv. Phys. 48 (1999) 167.
[9] S. Upadhyay, P. Kavitha, Mater. Lett. 61 (2007) 1912.
[10] S.V. Manorama, C.V.G. Reddy, V.J. Rao, Appl. Surf. Sci. 93 (2001) 174.
[11] M.V.R.A. Vegas, J.M. González-Calbet, M.A. Alario-Franco, Acta Cryst. B 42 (1986) 167.
[12] T. Endo, T. Masuda, H. Takizawa, M. Shimada, J. Mater. Sci. Lett. 11 (1992) 1330.
[13] K. Chiba, S. Makino, M. Mukaida, M. Kusunoki, S. Ohshima, Physica C 349 (2001) 35.
[14] M. Mukaida, M. Miura, A. Ichinose, K. Matsumoto, Y. Yoshida, S. Horii, A. Saito, F. Hirose, Y. Takahashi, S. Ohshima, Jpn. J. Appl. Phys. 44 (2005) 318.
[15] Q.Z. Liu, J.M. Dai, Z.L. Liu, X.B. Zhang, G.P. Zhu, G.H. Ding, J. Phys. D: Appl. Phys. 43 (2010) 455401.
[16] H.F. Wang, Q.Z. Liu, F. Chen, G.Y. Gao, W.B. Wu, X.H. Chen, J. Appl. Phys. 101 (2007) 106105.
[17] Q.Z. Liu, H.F. Wang, F. Chen, W.B. Wu, J. Appl. Phys. 103 (2008) 093709.
[18] C.C. Wang, G.Z. Liu, M. He, H.B. Lu, Appl. Phys. Lett. 92 (2008) 052905.
[19] X.N. Fu, Q.X. Yu, Q.Q. Gao, B. Chen, J. Appl. Phys. 111 (2012) 013907.
[20] P.L. Lang, Y.G. Zhao, B. Yang, X.L. Zhang, J. Li, P. Wang, D.N. Zheng, Appl. Phys. Lett. 87 (2005) 053502.
[21] Z.G. Sheng, W.H. Song, Y.P. Sun, J.R. Sun, B.G. Shen, Appl. Phys. Lett. 87 (2005) 032501.
[22] T.F. Zhou, G. Li, N.Y. Wang, B.M. Wang, X.G. Li, Y. Chen, Appl. Phys. Lett. 88 (2006) 232508.